

Exploring many-body localization in quantum systems coupled to an environment via Wegner-Wilson flows

Shane P. Kelly

*Theoretical Division, Los Alamos National Laboratory, Los Alamos, New Mexico 87545, USA
Physics and Astronomy Department, University of California Riverside, Riverside, California 92521, USA*

Rahul Nandkishore

*Department of Physics and Center for Theory of Quantum Matter, University of Colorado, Boulder, CO 80309, USA
Kavli Institute for Theoretical Physics, University of California, Santa Barbara, CA 93106-4030, USA*

Jamir Marino

*Department of Physics, Harvard University, Cambridge MA 02138, USA
Department of Quantum Matter Physics, University of Geneva, 1211, Geneva, Switzerland
Kavli Institute for Theoretical Physics, University of California, Santa Barbara, CA 93106-4030, USA*

Abstract

Inspired by recent experiments on many-body localized systems coupled to an environment, we apply a Flow Equation method to study the problem of a disorder chain of spinless fermions, coupled via density-density interactions to a second clean chain of spinless fermions. In particular, we focus on the conditions for the onset of a many-body localized phase in the clean sector of our model by proximity to the dirty one. We find that a many-body localization proximity effect in the clean component is established when the density of dirty fermions exceeds a threshold value. From the flow equation method we find that, similar to many-body localization in a single chain, the many-body localization proximity effect is also described by an extensive set of local integrals of motion. Furthermore, by tuning the geometry of the inter-chain couplings, we show that the dynamics of the model is ruled, on intermediate time scales, by an emergent set of quasi-conserved charges.

1. Introduction

The advent of cold gas experiments [1] has revitalized interest in fundamental questions of quantum thermodynamics in isolated many-body systems. One of the most intriguing avenues of research is the quest for non-ergodic phases of quantum matter. Examples range from integrable models [2, 3] to quantum scars [4] and include the prominent example of ergodicity breaking by strong disorder: many-body localization (MBL) [5, 6]

Email address: jamirmarino@fas.harvard.edu (Jamir Marino)

MBL has been the subject of intense research activity in the last ten years; seminal works have studied the problem both in a perturbation treatment [7, 8, 9] and with numerical methods [10, 11, 12], establishing that a localized phase, which exhibits absence of diffusion on long time scales, can survive the presence of many body interactions. Interest in many-body localisation results from its rich phenomenology: unusual dynamical responses [13, 14], a novel pattern of quantum entanglement [15, 16, 17, 18, 19], the possibility to host new types of order without equilibrium counterpart [20, 21, 22, 23], and connections to the notion of quantum integrability [15, 24, 25, 26, 27, 28, 29]. MBL systems possess an extensive set of quasi-local integrals of motion, conserved by the unitary dynamics, and preventing full thermalization. Such local degrees of freedom (called localized bits or l -bits) can be constructed via a sequence of local unitary transformations starting from a free Anderson insulator, and represents a form of quantum integrability robust to perturbations. This property is at the basis of a mathematical proof of the existence of the MBL phase for one-dimensional spin lattice systems with short-range interactions [30].

MBL is nowadays investigated in experiments with cold gases [31, 32, 33, 34] and superconducting qubits [35]. The advent of MBL in experimental platforms poses naturally the question of its robustness to the coupling with an external environment [36, 37]. A bath is expected to provide sufficient energy and phase-space to facilitate the hopping in an otherwise localized system [38, 39, 40, 41, 42, 43, 44, 45, 46]. On the other hand, a recent experiment [47] suggests that the clean 'environment' needs to reach a comparatively large density of particles with respect to the dirty MBL system in order to act as a thermodynamic environment and induce ergodic behavior. In order to render the problem treatable, the coupling between a quantum many body system and a bath is usually assumed weak. The complementary regime, however, presents an even more interesting scenario: when the back-action on the bath is strong, and the bath and system are of comparable size, the 'clean' bath could localize by proximity to the dirty system – a phenomenon called 'MBL proximity effect' [48, 49, 50].

Previous work has substantiated the existence of the 'MBL' proximity effect' via perturbative treatments [48, 50] and exact numerics on small system sizes [49], while to the best of our knowledge there has been no attempt at constructing integrals-of-motion, or an l -bit Hamiltonian, for 'MBL proximity' induced phases. Therefore, in this work we investigate the possibility of such a construction by use of the Wegner-Wilson flow equation method [51]. Similar to renormalization group approaches to the MBL problem [52, 53, 54, 55, 56, 57], the Wegner-Wilson flow equation method [51] constructs a set flow equations implementing infinitesimal stepwise diagonalization of the many-body Hamiltonian. When both the clean and dirty components of the system localize, these equations describe a unitary transformation, in both clean and dirty components, to an l -bit Hamiltonian which is diagonal in an extensive set of local conserved charges. By focusing on this regime, one can make an ansatz of the l -bit Hamiltonian that only includes a few relevant many-body terms. Thus, in addition to being able to study regimes of strong system-bath coupling, the flow equation method is also able to access system's sizes beyond those treatable in exact diagonalization, when disorder is sufficiently strong.

This approach allows us to establish the existence of the MBL proximity effect, and its consistency with a diagonal l -bit Hamiltonian of local conserved charges, in a wide range of parameters. Of particular note, we identify a regime for the MBL proximity effect complementary to the one explored in the experiment of Ref. [47]: above a certain critical density the dirty system acts effectively as a source of disorder and induces an MBL phase into the clean component. We also focus on novel physical regimes occurring when the geometry of the system-bath coupling is modified. Specifically, we consider the case of a dirty chain of fermions, coupled every $\delta > 1$

sites, to the clean one (see Fig. 6); the dirty chain acts as a distribution of impurities placed every δ sites, cutting the clean chain into a sequence of emergent integrals of motions. These conserved charges lead to non-ergodic dynamics on intermediate time scales but are destroyed when interactions between conserved charges becomes effective. At these longer time scales, instead, the dynamics cross over from non-ergodic behavior to thermal behavior.

1.1. Structure of the paper

We begin in section 2 with a review of the Wegner-Wilson flow Equation technique for a single chain and discuss how such a technique provides access to local conserved charges and an l -bit Hamiltonian. Then, in section 3, we generalize the approach for the two-chain problem and detail how to identify the parameter space where the MBL proximity effect is reliably described by an l -bit Hamiltonian. In section 4, we present the numerical solution to the flow equations in the case of two chains of equal length. Here, we demonstrate the stability of the MBL proximity effect, construct a qualitative phase diagram and present the numerically computed l -bit couplings. In section 5, we describe in greater detail the truncations made by the two-chain l -bit ansatz and sketch the derivation of the differential equations defining the FE unitary transformation. In section 6, we apply the method developed in the first sections to a novel geometry for the system-bath coupling, and discuss a novel relaxation process. We conclude with a quick overview on relevant experiments and possible future directions in section 7.

2. Flow Equation Approach For a Single Chain

The key idea of the FE approach is to introduce a family of unitary transformations, $U(l)$, parameterised by a 'renormalization group' scale, l , and generated by the anti-hermitian operator, $\eta(l)$, via the relation, $U(l) = T_l \exp(\int \eta(l) dl)$. The fixed point of the FE procedure in the $l \rightarrow \infty$ limit, is a diagonal Hamiltonian with dressed couplings. Operators, $O(l)$, flow according to the equation $\frac{dO}{dl} = [\eta(l), O(l)]$. A customary procedure for constructing $\eta(l)$ is to first separate the Hamiltonian into its diagonal, $H_0(l)$, and off-diagonal, $V(l)$ parts. Then, the generator is constructed as $\eta(l) \equiv [H_0(l), V(l)]$ which guarantees vanishing off-diagonal terms at the fixed point, $l \rightarrow \infty$ [58]. Typically, the solution of an interacting quantum many-body system via the FE approach would require a broad set of variational parameters keeping track of the nested hierarchies of multi-particles correlations.

However, in the case of MBL systems, a guiding insight in fixing the variational ansatz for the flow equations comes from the l-bit picture [59, 60], which provides a method to numerically solve the flow in an efficient way: only the first leading terms describing pairwise interactions between the l -bits are retained, while higher order effects are truncated and discarded. This represents an excellent description as long as the system is strongly localized. Given this ansatz for $H(l)$, the flow of the couplings is readily given by the solution of $\frac{dH}{dl} = [\eta(l), H(l)]$. In other words, the flow brings the Hamiltonian of a single disordered fermionic wire (for instance, H_d in Eq. (2)) into an effectively diagonal one at the fixed point

$$\mathcal{H}(\infty) = \sum_i h_i(\infty) n_i + \sum_{i,j} \Delta_{ij}(\infty) n_i n_j. \quad (1)$$

This, in turn, shows that the FE method effectively brings the Hamiltonian into an l-bit basis, with couplings between the integrals-of-motion that decay in space as $\Delta_{ij}(\infty)_{ij} \propto \exp(-|i-j|/\xi)$. The values of $h_i(\infty)$ and $\Delta_{ij}(\infty)$ depend on the specific disorder realization. Therefore, to

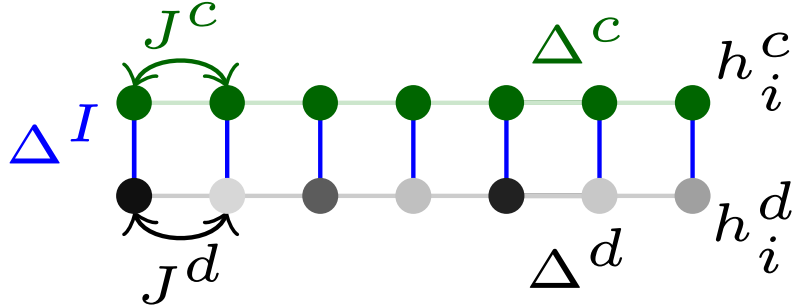


Figure 1: Cartoon of the model described by the Hamiltonian (2). The MBL sector (bottom wire) acts as a source of disorder to induce localization in the clean component (green sites). The two systems are coupled site by site via inter-chain couplings (blue lines) of strength Δ^I .

consider disorder averaged quantities, the flow equations must be computed independently for each disorder realization.

In addition to extracting the conserved charges and l-bit Hamiltonian in Eq. 1, the FE method can be used to approximate a crossover region from the MBL phase to a delocalized phase [60]. This region is identified with the parameter space where truncation error proliferates. These errors indicate the departure from an MBL phase because they indicate that the true unitary transformation must contain correlations between local degrees of freedom that are not captured by the ansatz. Since the growth of correlation between local degrees of freedom is suggestive of delocalization, the proliferation of truncation error is also indicative of a breakdown of the MBL phase. In order to measure the truncation error, one calculates the so-called 'second invariant' [60, 61], a quantity conserved by the exact unitary transformation. Since the truncation breaks the unitarity of the flow, the truncation error is controlled by changes in second invariant.

By setting a small threshold for the change in the second invariant, a tight bound on the MBL phase region can be identified with the parameter space where the truncation yields error within the threshold. Such analysis performed on the single chain led gives a phase boundary consistent with exact diagonalization [60]. We discuss the second invariant in detail as it pertains to the MBL proximity effect in section 3.3.

3. Flow Equation Approach For Two Chains

3.1. The model

In this section we extend the flow equation method to the system depicted in Fig. 1. We consider a system composed of two wires of interacting spinless fermions coupled via an inter-

chain density-density interaction of strength Δ^I . The Hamiltonian of the system reads (cf. Fig. 1)

$$\begin{aligned}
H &= H^c + H^d + H^I & (2) \\
H^c &= \sum_{ij} J_{ij}^c c_i^\dagger c_j + \sum_{ij} \Delta_{ij}^c n_i^c n_j^c \\
H^d &= \sum_{ij} J_{ij}^d d_i^\dagger d_j + \sum_{ij} \Delta_{ij}^d n_i^d n_j^d + \sum_k h_i n_i^d \\
H^I &= \sum_{ij} \Delta_{ij}^I n_i^c n_j^d
\end{aligned}$$

where the sums run over N_s dirty sites in the Hamiltonian H^d and over $\delta \times N_s$ clean sites (with $\delta \geq 1$) in the Hamiltonian H^c . The fields, h_i , are drawn from a uniform box distribution of variance W , i.e. $h_i \in [-W, W]$; for sufficiently large W , the chain of fermions, d_i , will be in the MBL phase, and will act on the clean fermionic component, c_i , as a source of disorder. Even though we study a microscopic model that contains inhomogeneities only in the on-site fields, h_i , we write couplings in Eq. (2) with a generic dependence on spatial indices to emphasize that, already at the first steps of integration of the flow equations, couplings can inherit an explicit spatial dependence from the disordered fields.

3.2. Two Chain Ansatz

Similar to the FE method for single chain MBL phase, the FE method for the two-chain problem aims to construct a unitary transformation, $U(l) = T_l \exp(\int \eta(l) dl)$, that diagonalizes the Hamiltonian Eq. 2. In both cases, an exact calculation would require keeping track of $O(2^{N_s^2})$ matrix elements and is therefore numerically unfeasible. As for the MBL phase in the single chain problem, the local nature of the MBL proximity effect allows one to circumvent this issue via an ansatz for the Hamiltonian, $H(l) = U^\dagger(l) H U(l)$ at scale l of the unitary transform. The ansatz we use for the two-chain problem is $H(l) = H_0(l) + V(l)$ where

$$\begin{aligned}
H_0(l) &= H^c(l) + H^d(l) + H^I(l) & (3) \\
H^c(l) &= \sum_{ij} \Delta_{ij}^c(l) : n_i^c n_j^c : + \sum_k \bar{h}_k^c(l) : n_k^c : \\
H^d(l) &= \sum_{ij} \Delta_{ij}^d(l) : n_i^d n_j^d : + \sum_k \bar{h}_k^d(l) : n_k^d : \\
H^I(l) &= \sum_{ij} \Delta_{ij}^I(l) : n_i^c n_j^d : \\
V(l) &= \sum_{ij} J_{ij}^c(l) : c_i^\dagger c_j : + \sum_{ij} J_{ij}^d(l) : d_i^\dagger d_j,
\end{aligned}$$

: A : denotes Wick Ordering [51], the fields $\bar{h}^{c(d)}$ are given below in Eqs. (4), and we will use the convention that the first index in Δ_{ij}^I refers to the clean chain. In the limit $l \rightarrow \infty$, $V(l) \rightarrow 0$, the fixed-point Hamiltonian, $H(l \rightarrow \infty)$, is diagonal in an extensive set of 1-bits localized on both the clean and dirty sites.

As customary for flow equation methods [60, 51], we use Wick-ordered operators, : A :, with respect to a reference state ρ . Wick ordering reduces errors in the truncated Hamiltonian $H(l)$ for the Hilbert space spanned by few particle excitations on top of the reference state ρ [51]. As done

by Thomson *et al.* in [60], we choose a reference state with zero entanglement between local degrees of freedom. This extreme locality condition serves a starting point for the FE unitary transformation to capture the entanglement of the MBL proximity effect. The state ρ employed is a Boltzmann distribution, $\rho = \frac{1}{Z} e^{-\Theta H_w}$, with inverse temperature Θ , chemical potentials fixing particle densities $\langle n^d \rangle$ and $\langle n^c \rangle$, and Hamiltonian $H_w = \sum_i (h_i^d - \mu^d) n_i^d - \mu^c n_i^c$. The choice of this state allows to easily control energy density, Θ , and particle density distribution, $\langle n^d \rangle$.

By Wick-ordering the Hamiltonian at flow time $l = 0$, the clean and dirty chains pick up effective fields, given by

$$\begin{aligned}\bar{h}_i^d &= h_i^d + 2 \sum_j \Delta_{ij}^d \langle n_j^d \rangle + \sum_j \Delta_{ji}^I \langle n_j^c \rangle, \\ \bar{h}_i^c &= 2 \sum_j \Delta_{ij}^c \langle n_j^c \rangle + \sum_j \Delta_{ij}^I \langle n_j^d \rangle;\end{aligned}\tag{4}$$

where their distribution depends on the dirty chain density, $\langle n^d \rangle$, the inter-chain coupling Δ^I , and the disorder, W , in the dirty chain. From the expressions of the fields in Eq. (4), it is natural to observe that, if the dirty chain is sufficiently disordered and the inter-chain couplings are sizable, the clean chain will localize as result of the effective disordered field, \bar{h}_i^c .

Note, the ansatz in (3) has the notational symmetry

$$\begin{aligned}c &\leftrightarrow d \\ \Delta_{ij}^I &\leftrightarrow \Delta_{ji}^I.\end{aligned}\tag{5}$$

By exploiting this symmetry, it is easy to derive flow equations for operators of the dirty chain from those of the clean one, and vice-versa. We will refer to terms (or equations) produced by such symmetry transformations using the notion $C \leftrightarrow D$ in the following.

3.3. Second Invariant and Phase Boundary Analysis

From the ansatz in Eq. 3, we can derive the FE generator $\eta(l) = [H_0(l), V(l)]$. Then, by matching the truncated terms in the Heisenberg equation of motion, $dH(l)/dl = [\eta(l), H(l)]$, the *truncated flow equations*, a set of first order differential equations for the couplings,

$$\Gamma = \{\Delta_{ij}(l)^{c(d,I)}, J_{ij}^{c(d)}(l), \bar{h}_k^{c(d)}(l)\},\tag{6}$$

can be derived

$$\frac{d\Gamma}{dl} = \beta(\Gamma),\tag{7}$$

where the β functions are order three polynomials in the couplings Γ and their forms discussed in detail in section 5. An l -bit Hamiltonian, $H(l \rightarrow \infty)$, is retrieved by numerically evolving Eq. 7 with initial conditions given by the bare physical couplings, evolved for large l . Deep in the MBL proximity effect phase, these differential equations describe a unitary transform to a diagonal Hamiltonian $H(l \rightarrow \infty)$, and the unitary transformation described by $\eta(l)$, along with the Hamiltonian $H(\infty)$, can be used to predict dynamics of relevant observables [60, 51, 62].

When either chain delocalizes, the l -bit Hamiltonian ansatz will be an insufficient representation of the effective Hamiltonian, and the couplings $\eta(l)$ and $H(\infty)$ cannot be used to make

predictions. To detect the breakdown of the MBL proximity effect ansatz, we monitor the extent that the truncated flow equations, Eq. 7, break unitarity. For this goal, we employ a quantity known as the second invariant, see, for instance, previous work in Refs. [60, 61]. The second invariant is the $p = 2$ case of a class of many invariants of the FE unitary transformation given by $\text{Tr}[H(l)^p]$. It is particularly easy to calculate for the spin systems and is given by:

$$\text{Tr} [H(l)^2] = \sum_{ij,r=c,d} (J_{ij}^r)^2 + (\Delta_{ij}^r)^2 + \Delta_{ij}^I + \sum_{k,r=c,d} (\bar{h}_k^r)^2. \quad (8)$$

We can then quantify the error made by a given ansatz by computing the change in the second invariant:

$$\delta I = 2 \frac{\text{Tr} [H(l = \infty)^2] - \text{Tr} [H(l = 0)^2]}{\text{Tr} [H(l = \infty)^2] + \text{Tr} [H(l = 0)^2]}. \quad (9)$$

If δI is small, then the MBL proximity effect ansatz in Eq. 3, and the approximations discussed above, represent a reliable description and can be used to compute dynamics and the local conserved l-bits. On the other hand, when δI is large, we have an indication that the ansatz fails and that we cannot use the generator $\eta(l)$ nor the l-bit Hamiltonian $H(\infty)$ to make predictions.

By identifying a threshold for δI , we can find a tight bound on the phase boundary for the MBL proximity effect. While the choice of threshold is arbitrary, by making it stringently small, one can ensure that below that threshold the MBL proximity effect is properly captured. On the other hand, if it is above that threshold, we must conclude that 1) the system is delocalized or, 2) it is localized in an operator basis not captured by the ansatz. If 2) is the case, then, the operator basis must contain either non-local operators or operators capturing stronger correlations. In either case, a reasonably chosen threshold should yield an approximate boundary for the MBL proximity effect.

4. Numerical Results For Equal Length Chains

4.1. MBL Proximity Effect

In this section, we present numerical results, for system sizes unattainable with exact diagonalization, that establish the validity of using an l-bit Hamiltonian to describe the MBL proximity effect. We study the model introduced in section 3.1 for two equal length chains of length $N_s = 24$ (48 total sites), and numerically solve the differential flow equations, Eq. 7. For this model, the initial couplings are given as:

$$\begin{aligned} \Gamma(l = 0) = & \quad (10) \\ \left\{ \begin{aligned} \Delta_{ij}^{c(d)}(l = 0) &= \Delta^{c(d)}(\delta_{i,j+1} + \delta_{j,i+1}), \\ \Delta_{ij}^I(l = 0) &= \Delta^I \delta_{ij}, \\ J_{ij}^{c(d)}(l = 0) &= J^{c(d)}(\delta_{i,j+1} + \delta_{j,i+1}), \\ \bar{h}_i^d(l = 0) &= h_i^d + 2 \sum_j \Delta_{ij}^d(l = 0) \langle n_j^d \rangle + \sum_j \Delta_{ji}^I(l = 0) \langle n_j^c \rangle, \\ \bar{h}_i^c(l = 0) &= 2 \sum_j \Delta_{ij}^c(l = 0) \langle n_j^c \rangle + \sum_j \Delta_{ij}^I(l = 0) \langle n_j^d \rangle \end{aligned} \right\} \end{aligned}$$

where h_i^d is drawn from a box distribution in the interval, $[-W, W]$, and clean and dirty number densities are computed with respect to the Wick ordering reference state, $\langle n_k^{c(d)} \rangle = \text{Tr}[\rho n_k^{c(d)}]$. We focus on the limit in which the disordered system would be strongly localized and vary the inter-chain coupling, clean chain hopping strength and reference state parameters. Therefore, we set $W = 60$, $\Delta^d = J^d = 0.1$, and vary the parameters Δ^I , J^c , $\langle n^d \rangle$ (μ^d) and Θ . By setting $\Delta^c = 0.1$, we also focus our attention to the limit in which the clean intra-chain coupling is weak.

The exact form of the truncated flow-equations are given in [Appendix C](#) and discussed in section 5. For a fixed configuration of h_i^d , the truncated flow equations are numerically evolved for a sufficiently long flow-time such that 1) the hoppings, $J_{ij}^{c(d)}(l)$, have become sufficiently small, and 2) there is no appreciable change in the flow of any other coupling. The evolution is repeated for different random instances of h_i^d , and we present the disorder average of the asymptotic ($l \rightarrow \infty$) couplings.

In analogy to a single disordered chain, we define an effective disorder parameter as $W^c = \Delta^I/2J^c$ and work in a limit in which the clean chain is expected to be strongly localized: $\Delta^I = 45$, $J^c = 0.1$, $\Theta = 0.3$ and $\langle n^d \rangle = 0.5$ (i.e. $W^c = 225$). We choose such a strong effective disorder to benchmark the method and isolate the effects of varying different parameters. Solving the numerical flow equations (see [Appendix D](#) for details on numerical implementation), we find that the density-density couplings, $\Delta_{ij}^{c(d)}$, are exponentially suppressed in $|i - j|$, as it occurs in the applications of the Wegner flow to single disordered chains[59, 60]. In Fig. 2a, we show the decay in space of the disorder-averaged, asymptotic, density-density couplings, $\Delta_{ij}^c(l \rightarrow \infty)$, on a logarithmic scale, and they illustrate the onset of an MBL phase in the clean chain. As discussed below, the change in the second invariant for these parameters is small for the majority of disorder realizations and thus confirms the validity of the MBL proximity effect ansatz employed in this ansatz.

The top panel of Fig. 2 shows that by decreasing the inter-chain coupling, the final density-density couplings between the l -bits present a slower decay in space suggesting a departure from the MBL proximity phase. The effective disorder parameter, $W^c = \Delta^I/2J^c$, can be used to compare with the disordered Heisenberg chain (a prototype of MBL), which shows a transition at $W/J = 4$. By considering the second-invariant, we find that the truncation produces minimal error for $W^c \gtrsim 10$ and the MBL proximity is well-established. Note that while we benchmark the method with $W^c = 225$, we found the MBL proximity effect to be consistent with a l -bit ansatz for a reasonable effective disorder strength of $W^c > 10$. While for $W^c \lesssim 10$, the error grows with decreasing W^c and suggests that somewhere in the range $W^c \lesssim 10$ the system undergoes a transition to a delocalized phase. In this limit, we have found that the final density-density couplings for the dirty-chain, $\tilde{\Delta}_{ij}^d$, are still strongly localized while those for the clean-chain are not. This suggests that the source of truncation error is due to the clean-chain becoming delocalized.

The bottom panel of Fig. 2b is one of the most interesting results of our analysis. Here, different curves correspond to different fermionic densities of the dirty component in Hamiltonian (2), with fixed total fermionic density, $\langle n_{tot} \rangle \equiv \langle n^d \rangle + \langle n^c \rangle = 0.5$. This variation of $\langle n^d \rangle$ follows a similar logic to the experiment in Ref. [63], where a complementary situation has been considered (the melting of an MBL phase by coupling to a clean bath). There, the delocalizing effect of the clean component on the dirty component has been experimentally observed in a mixture of collisionally coupled ultra-cold bosons in a two-dimensional optical lattice. Above a certain critical density of bosons, the clean component acts as an ergodic bath and destroys the features

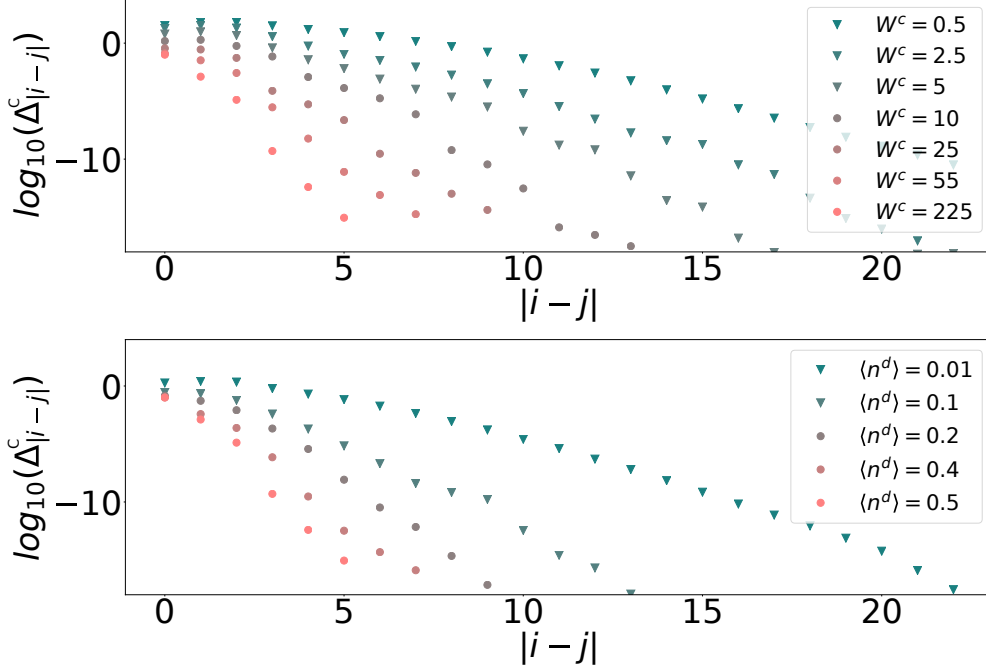


Figure 2: Instances of the MBL proximity effect: the plots show, in logarithmic scale, the spatial decay of the couplings between integrals of motion in the clean sector of the system. We display results for parameters which yield both a large and small change in the second invariant, and distinguish them using triangle and circle markers respectively. The results for parameters that yielded a large change in the second invariant (marked with triangles) do not reflect the true 1-bit coupling but are displayed to depict how the MBL proximity effect ansatz breaks down. The final clean-chain density-density couplings $\Delta_{|i-j|}^c$ depicted here are averaged over 256 disorder realizations. In the top panel, we plot how the final density-density couplings depend on $W^c = \Delta^I/2J^c$ (J^c fixed) while in the bottom panel we plot their dependence on $\langle n^d \rangle$. In the top panel $\langle n^d \rangle = 0.5$ while in the bottom panel $W^c = 225$ ($\Delta^I = 45$ and $J^c = 0.1$). The remaining Hamiltonian parameters are $W = 60$, $J^d = \Delta^d = 0.1$, $\Delta^c = J^c = 0.1$, $\Theta = 0.3$, and $\langle n^c \rangle = 0.1$. These results are not affected by $\langle n^c \rangle$ since they are uniformly distributed in the reference state ρ and do not have an impact on the disorder of the effective fields.

of the MBL phase in the dirty sector. Complementary, we find that a critical density of dirty fermions is required in order for the MBL systems to be sufficiently large to entail localization in the clean component. The analysis of the second invariant identifies that the MBL proximity effect is well-established for $\langle n^d \rangle > 0.25$, and suggests that for some value of $\langle n^d \rangle$ less than 0.25, the clean chain goes through a delocalization transition. It is important to note that we are unable to identify with accuracy the point of transition since our ansatz fails close to it (see also Ref. [60]).

We have also studied the effect of increasing the clean-chain hopping, J^c and the energy density parameterised by the inverse temperature, Θ of the reference state ρ . We found that the 1-bit ansatz, Eq. 3, becomes inefficient for large clean chain hopping, $J^c > 0.5$, and at large energy densities, $\Theta < 0.05$. In these limits, the clean chain couplings, Δ_{ij}^c , begin to delocalize while the dirty chain couplings, Δ_{ij}^d , are unaffected. This dependence of localization on the hopping strength is similar to a standard MBL system (the system delocalizes at strong hopping), while

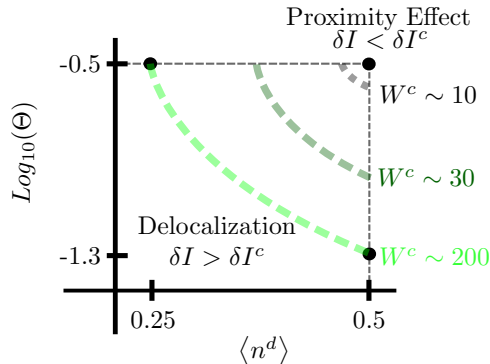


Figure 3: Regions of parameter space where the MBL proximity effect is established. We focus on an instance of a strongly localized dirty chain ($W = 60$, $\Delta^d = J^d = 0.1$), and on a clean chain with $\Delta^c = J^c = 0.1$. The thin, dashed, black lines delimit a square where the parameters Θ and $\langle n^d \rangle$ have been varied in our numerical trials. The region of parameters space in which the MBL Proximity Effect is established is determined by the region where the second invariant is below a specified threshold $\delta I < \delta I^c = 0.1$. In the figure, we draw three different thick, curved, dashed lines, corresponding to the values of the parameter $W^c = 10$ (gray), 30 (dark green), 200 (bright green). These lines mark the values of Θ and $\langle n^d \rangle$ where we expect the second invariant to equal the threshold value $\delta I(W^c, \langle n^d \rangle, \Theta) = \delta I^c$, and above which we expect $\delta I(W^c, \langle n^d \rangle, \Theta) > \delta I^c$. This analysis demonstrates that the MBL Proximity Effect can be observed for the smaller $\langle n^d \rangle$ and Θ when W^c is larger.

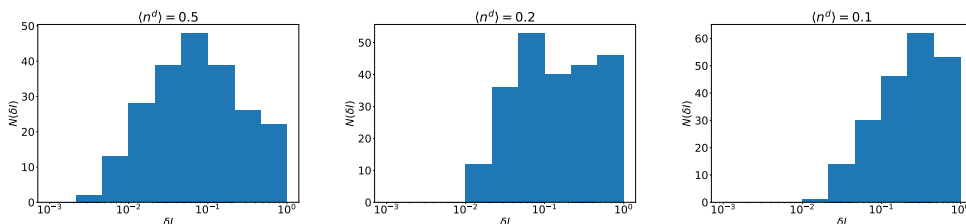


Figure 4: Histograms of the change in the second invariant as $\langle n^d \rangle$ is varied across the transition ($W = 60$, $J^d = \Delta^d = 0.1$, $\Delta^c = J^c = 0.1$, $\Theta = 0.3$, and $\langle n^c \rangle = 0.1$).

the dependence on the energy density of the dirty chain is novel. At low energy density, the dirty chain charge distribution in the reference state, $\langle n_k^d \rangle$, and, correspondingly, the effective clean disorder fields, \bar{h}_k^c , are strongly disordered, and the clean chain localizes. While for high energy density, the reference state has no disorder in the dirty chain densities, and the clean chain delocalizes. Extrapolating these results, we expect that the localization of the clean chain depends on the disorder of the dirty chain charge distribution.

We summarize our results in the portrait of Fig. 3, which shows the region of the Θ - $\langle n^d \rangle$ plane where the change in the second invariant is expected to be smaller than our chosen threshold $\delta I^c = 0.1$. In addition to depicting the trends just discussed, it shows that the dirty chain densities of the reference state must be strongly disorder to compensate for a weaker inter-chain coupling $\Delta^I (W^c)$, in order to induce MBL in the clean sector.

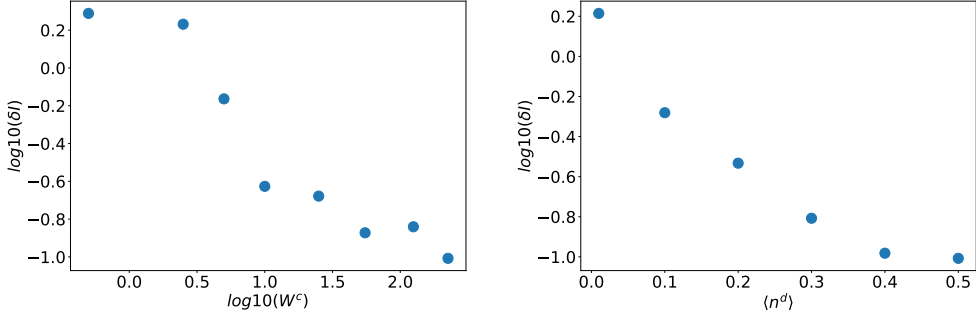


Figure 5: Median change in the second invariant as a function of $\langle n^d \rangle$ (right) and of W^c (left). W^c is plotted on a log scale since it varies over two orders of magnitude. The remaining Hamiltonian parameters are $\Delta^I = 45$ ($W^c = 225$), $J^d = \Delta^d = 0.1$, $\Delta^c = J^c = 0.1$, $\Theta = 0.3$, and $\langle n^c \rangle = 0.1$. In the left panel $\langle n^d \rangle = 0.5$, while, on the right panel, $W^c = 225$ ($\Delta^I = 45$).

4.2. Second Invariant

Above we used the second invariant, δI , to identify when the truncated flow equations preserve the unitarity of the exact Wegner-Wilson flow and to justify the MBL-proximity effect ansatz, Eq. 3. Because the flow equation transformation depends on the disorder realization, δI varies from sample-to-sample. The left panel of Fig. 4 shows the distribution of δI for a disorder strength where the MBL-proximity effect ansatz is valid for the majority of disorder realizations, while the right panel shows the distribution for a system where the same ansatz fails for the majority of disorder realizations. In order to distinguish between these two situations, we can compute the median of δI (we don't use the mean because it is artificially biased by the few trials with large second invariant weight). As shown in Fig. 5, the median δI shows that the MBL proximity effect ansatz becomes worse for decreasing Δ^I and $\langle n^D \rangle$. Here we see that for $W^c > 10$ and for $\langle n^d \rangle > 0.25$, the median second invariant is small and relatively unaffected by changes in W^c and $\langle n^d \rangle$, demonstrating the validity of the MBL proximity effect ansatz. While for small $W^c < 10$ and small $\langle n^d \rangle < 0.25$, the error made by truncation is large and suggestive of a transition to delocalization somewhere below these values. The large sample-to-sample variation of the second invariant suggests the presence of regions not captured by the MBL proximity effect ansatz, and future work may attempt to reduce the second invariant for these disorder realizations by improving the ansatz.

5. Truncated Flow Equations and Truncation Error

5.1. Truncation Error for the MBL Proximity Effect Ansatz

In the previous section we have shown that the l -bit ansatz, Eq. 3, accurately describes the MBL proximity effect phase and that the truncated flow equations, Eq. 7, imply a small error in approximating the exact flow equation unitary transformation, $U(l)$. In this section, we analyze the approximations made by the truncation in Eq. 3, and we discuss, in section 5.2, the physics of the terms contributing to the truncated flow equations. The first type of operators dropped are the $n > 2$ body terms such as the three body scattering, $: c_i^\dagger c_j^\dagger c_k^\dagger c_i c_j c_k :.$ As long as the integrals of motion do not contain $n > 3$ body operators with significant weight, then truncating these terms

will not produce significant error in the integrals of motion, FE unitary transformation, or l -bit Hamiltonian. This is confirmed by the small second invariant presented in the previous section. It is important to note that, despite dropping these n -body scattering operators, the ansatz does not ignore all n -body correlations: while at scale l the few body terms are not $n > 3$ body correlated in the transformed basis, they do contain $n > 3$ correlations in the physical basis (i.e. $U(l) : c_i^\dagger(l)c_j(l) : U^\dagger(l)$ contains n -body operators).

In addition to dropping $n > 3$ body scattering operators from the l -bit ansatz, we drop the off-diagonal terms : $n_k^c c_i^\dagger c_j$: and : $c_k^\dagger c_l c_i^\dagger c_j$:, which we will call correlated hopping and full two-body scattering (F.S) respectively. Including these terms requires keeping track of $O(N_s^3)$ ($O(N_s^4)$ for F.S.) number of couplings and significantly increases the computational resources required. To identify the error produced by dropping these terms we highlight how they are produced as the flow evolves.

We identify 7 distinct operators by the 7 sums shown in Eq 3:

$$\begin{aligned} H^c(l) &= \hat{\Delta}^c + \hat{h}^c \\ H^d(l) &= \hat{\Delta}^d + \hat{h}^d, \\ H^I(l) &= \hat{\Delta}^I \\ V(l) &= \hat{J}^c + \hat{J}^d \end{aligned} \quad (11)$$

where, $\hat{h}^c = \sum_k \bar{h}_k^c : n_k^c$:, $\hat{J}^c = \sum_{ij} J_{ij}^c(l) : c_i^\dagger c_j$:, etc. (see Appendix A for explicit forms for the remaining operators). We then classify contributions to the generator by the type of off-diagonal operator appearing in the commutator: $\eta = [H_0, J] = \eta_h + \eta_\Delta + \eta_I$ where:

$$\begin{aligned} \eta_h &= [\hat{J}^c, \hat{h}^c] + [\hat{J}^d, \hat{h}^d] \\ \eta_\Delta &= [\hat{J}^c, \hat{\Delta}^c] + [\hat{J}^d, \hat{\Delta}^d] \\ \eta_I &= [\hat{J}^c + \hat{J}^d, \hat{\Delta}^I]. \end{aligned} \quad (12)$$

These commutators are computed using rules for Wick ordering [51] and yield:

$$\begin{aligned} \eta_h &= \sum_{ij} F_{ij} : c_i^\dagger c_j : + C \leftrightarrow D \\ \eta_\Delta &= \sum_{ijk} \Gamma_{ij|k}^c : n_k^c c_i^\dagger c_j : + F_{ij}^\Delta : c_i^\dagger c_j : + C \leftrightarrow D \\ \eta_I &= \sum_{ijk} \Gamma_{ij|k}^I : n_k^d c_i^\dagger c_j : + C \leftrightarrow D \end{aligned} \quad (13)$$

where the coefficients Γ and F are given in Appendix B. The form of the generators are either a hopping operator, : $c_j^\dagger c_i$:, a correlated hopping (C.H) operator, : $n_k^c c_i^\dagger c_j$: or an inter-chain correlated hopping (C.H.I) operator : $n_k^c c_i^\dagger c_j$:. It will be important for quantifying the error implied by our truncation to notice that each of the generators is proportional to J_{ij}^c or J_{ij}^d . In addition, the η_Δ generator is also proportional to $\Delta_{ij}^{c(d)}$.

Taking the commutator $[\eta(l), H_0(l) + V(l)]$ yields contributions contained both inside and outside the ansatz, $H(l)$, and are summarized in Table. 1. The operators outside the ansatz are dropped and produce errors proportional to their coefficients. We expect the majority of these coefficients to be small because we study the MBL proximity effect in a limit that the couplings

	$\hat{h}^{c(d)}$	$\hat{J}^{c(d)}$	$\hat{\Delta}^{c(d)}$	$\hat{\Delta}^I$
η_h	$J_{ij}^{c(d)}$	$J_{ij}^{c(d)}, \hat{h}_i^{c(d)}$	C.H. $J_{ij}^{c(d)}$	C.H.I
η_Δ	C.H.	$\Delta_{ij}^{c(d)}, \text{C.H.}, \text{F.S.}$ $J_{ij}^{c(d)}, \hat{h}_i^{c(d)}$	3P C.H. $J_{ij}^{c(d)}$	3P C.H.I
η_I	C.H.I	$\Delta_{ij}^I, \text{C.H.I.}, \text{F.S.I}$ $J_{ij}^{d(c)}, \hat{h}_i^{d(c)}$	3P C.H.	3P C.H.I $J_{ij}^{c(d)}$

Table 1: This table lists which terms in the commutator $[\eta, H]$ contribute to the beta function $\beta(\Gamma)$ (highlighted in blue) and which are dropped by our ansatz (not highlighted). The rows are labeled by the terms in the sum for the generator $\eta = \eta_h + \eta_\Delta + \eta_I$, and the columns are labeled by the terms in the sum for the Hamiltonian, Eq. 11. The notation for the dropped terms is as follows: correlated hopping (C.H.) have a form $n_k^c c_i^\dagger c_j$, inter-chain correlated hopping operators C.H.I. have a form $n_k^d c_i^\dagger c_j$, full scattering terms F.S. have a form $c_i^\dagger c_j^\dagger c_k c_l$, and 3P terms describing three-body and higher particle scattering. The justification for dropping the contributions to $J_{ij}^{c(d)}$ in the third and fourth column is discussed in section 5.2.

$\Delta_{ij}^{c(d)}$ and $J_{ij}^{c(d)}$ are initialized as small. For example, operators appearing in the second row and second and third column appear with coefficients that are proportional to the square of these couplings, and since they are initialized with $\Delta^{c(d)} = J^{c(d)} = 0.1$ the error made is $O(0.01)$.

Besides these operators, there are still a few that appear linear in a small coupling and could produce larger error. For example, $[\eta^I, \hat{h}^c]$ produces an inter-chain correlated hopping operator, $n_k c_i^\dagger c_j$, which has a coefficient proportional to $J^c (\Delta^I)^2$. While this off-diagonal operator is not small, it is initialized to zero and only affects the diagonal Hamiltonian after commuting with a generator that is also proportional to J^c . Therefore, its effect on the diagonal Hamiltonian will remain small as long as J^c remains small. This is confirmed by the small change in the second invariant presented above.

This completes our analysis of the error produced by the truncation in the Ansatz, Eq. 3. In summary, we have discussed how we expect that a small error will be produced in our truncation scheme, as long as $\Delta^{c(d)}$ and $J^{c(d)}$ are initialized to small values. We then referenced results in section 4, which demonstrate small truncation error via a small change in the second invariant, to confirm such expectations.

5.2. Truncated Flow Equations

In the previous section, we have sketched the derivation of the FE Heisenberg equation of motion, $\frac{d\hat{H}}{dt} = [\eta(l), H(l)]$, and discussed the error produced by the truncation of the ansatz. In this section we focus on operators in $[\eta(l), H(l)]$ that contribute to the ansatz and truncated flow equations (Eq. 7). We first focus on the contribution in first row, first column of table 1. For the clean chain it produces a term:

$$\begin{aligned}
[\eta_h, \hat{h}] = & \left[\left[\hat{J}^c, \hat{h}^c \right], \hat{h}^c \right] + \dots = \\
& -J_{ij}^c (\bar{h}_i^c - \bar{h}_j^c)^2 : c_i^\dagger c_j + \dots
\end{aligned} \tag{14}$$

and therefore contributes to the evolution of J_{ij}^c :

$$\frac{dJ_{ij}^c}{dl} = -J_{ij}^c(\bar{h}_i^c - \bar{h}_j^c)^2 + \dots \quad (15)$$

This is the primary contribution evolving the off diagonal terms to 0, and is responsible for the intuitive physics discussed above. If we ignore the other contributions to dJ_{ij}^c/dl then the evolution of J_{ij}^c is:

$$J_{ij}^c(l) = J_{ij}^c(l=0)e^{-(\bar{h}_i^c - \bar{h}_j^c)^2 l}. \quad (16)$$

Thus, the stronger the disorder in the effective fields \bar{h}_i^c , the faster the off diagonal terms decay.

In addition to producing terms in the β functions that removes the off diagonal couplings J_{ij}^c , the generator η_h renormalizes $\hat{h}^{c(d)}$ and generates off diagonal hoppings $J_{ij}^{c(d)}$ at intermediate scales l of the FE evolution. These terms come from the first row, second column of table. 1 and have a characteristic contribution, $[\eta_h, \hat{J}^c] = \left[\left[\hat{J}^c, \hat{h}^c \right], \hat{J}^c \right] + \dots$, which produces contributions to the truncated flow equations as:

$$\begin{aligned} \frac{d\bar{h}_k^c}{dl} &= \sum_i 2(J_{ik}^c)^2(\bar{h}_k^c - \bar{h}_i^c) + \dots \\ \frac{dJ_{ij}^c}{dl} &= -\sum_k J_{ik}^c J_{kj}^c (2\bar{h}_k^c - \bar{h}_i^c - \bar{h}_j^c) + \dots \end{aligned} \quad (17)$$

Together with Eq. 15, Eq. 17 highlights the physics contained in the unitary transformation generated by η_h : The generator η_h is constructed to remove hoppings $J_{ij}^{c(d)}$ that change the energy of the diagonal Hamiltonian, H_0 , due to the effective fields $\bar{h}_k^{c(d)}$. Eq. 15 shows that the contribution from the commutator $[\eta_h, \hat{h}^c]$ removes off diagonal couplings, while Eq. 17 captures new terms produced by the rotation by η_h .

Similar physics occurs for the generators η_Δ and η_I , which are constructed to remove hoppings that change energy via the density-density interaction. In a strong interacting limit, the exact unitaries produced by these generators will generate a Hamiltonian describing doublon and domain wall propagation[64]. If disorder is also strong, these quasi-particle excitation may also localize, realizing a novel MBL of correlated quasi-particles. Unfortunately, in order to capture these effects, one needs to keep track of computationally demanding correlated hopping operators [64] dropped by our ansatz.

While such considerations offer promising prospects for future work, they also have direct consequences for the contributions we include in the truncated flow equations. Since the generators η_Δ and η_I transform the hopping operators, $\hat{J}^{c(d)}$, into a set of correlated hopping operators that commute with density-density interactions [64], the truncation above yields a transformation which simply removes the hopping operators without producing the correlated hopping operators they transform into. If these correlated hopping operators are responsible for delocalization, then removing them would produce an artificial localization. To avoid this false localization, we remove the contribution to $\frac{d}{dl}J_{ij}^{c(d)}$ coming from $[\eta_\Delta, \Delta]$ and $[\eta_I, \Delta^I]$ (respectively, second row, third column; and third row, fourth column; of table 1). Ignoring these contributions only produces small error for the same reason dropping the correlated hopping operators produces small error:

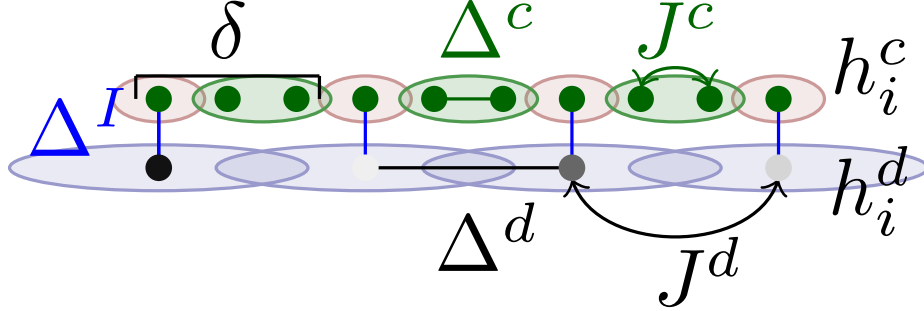


Figure 6: The dirty chain couples to the clean chain every $\delta = 3$ sites. The emergent integrals of motion are illustrated with different colors: n_k^d (blue), $n_{f,r=0}^c$ (red) and N_f (green).

the error in J_{ij} is proportional to $J_{ij}^{c(d)}$ but its contribution to the l -bit Hamiltonian is $(J_{ij}^{c(d)})^2$. The small error is numerically confirmed by a small second invariant as discussed above.

The remaining contributions from η_Δ and η_I are the ones in the second column of table 1 and describe delocalization processes produced by density-density interactions. A characteristic contribution is:

$$[[\hat{J}^c, \hat{\Delta}^c], \hat{J}^c], \quad (18)$$

which produce a contribution to the evolution of Δ_{ij}^c as:

$$\frac{d\Delta_{ij}^c}{dl} = 2 \sum_{k \neq i, j, l=i, j} J_{lk}^2 (\Delta_{ij}^c - \Delta_{kl}^c). \quad (19)$$

This contribution captures how the truncated flow equations break the unitary character of the FE transform in a delocalized limit. When disorder is small, J_{ij} remains finite longer during the flow equation evolution and Δ_{ij}^c has a longer time to grow according to the contribution in Eq. 19. This growth produces larger truncation error because, as discussed in the previous section, truncation error is only small when Δ_{ij}^c is small. This concludes our analysis of the physical content of the contributions to the truncated flow equations. The full set of truncated flow equations used in our numerics are reported in Appendix C.

6. Engineering the geometry of the inter-chain couplings

We now discuss novel effects arising by tuning the coupling geometry. In the geometry of Fig. 6 each fermion of the dirty chain is coupled, every δ sites, to a fermion of the clean chain. This new geometry can still be studied using analogous flow equations to those employed above. Since the clean chain is δ times longer than the dirty chain, we can label the dirty chain with $f = 0 \dots N_s - 1$, and conveniently reference the sites of the clean chain ($k = 0 \dots N_s \delta - 1$) with r , using $k = f\delta + r$. f labels the dirty sites, and $r = 0 \dots \delta - 1$ is the number of sites away from the coupled site. We can now explicitly write the initial inter-chain coupling as $\Delta_{f,r,f'} = \Delta^I \delta_{f,f'} \delta_{r,0}$. This leads to an initial clean-chain effective field of $\bar{h}_{f,r}^c = \Delta^I \langle n_f^d \rangle \delta_{r,0}$.

With this important modifications, we can straightforwardly evolve the couplings using the same truncated flow equations discussed in the previous sections. We show evolution of few of them in Fig. 7. The right panel of Fig. 7 shows the suppression of the hopping between a coupled site $f, r = 0$ and an uncoupled site $f, r = 1$, while the left panel of Fig. 7 shows the hopping between two uncoupled sites, $f, r = 1$ and $f' = f, r = 2$, remaining constant. This is consistent with the expectations given by Eq. 16: for a particle to hop on to a coupled site its energy must change by $(\bar{h}_i^c - \bar{h}_j^c) \approx \Delta^I \langle n^d \rangle$, while such a change of energy is not required for a particle hopping between two uncoupled sites.

With the hopping between uncoupled sites remaining constant, Eq. 19 predicts the divergence of the associated density-density couplings. This is depicted in the left panel of Fig. 7 and explains the failure of the MBL proximity effect ansatz. Instead of modifying the ansatz, we propose to modify the generator, $\eta(l)$ of the unitary transformation. We define a modified generator $\eta' = [H_0, V']$, where we choose V' to only include hoppings to coupled sites:

$$V'(l) = \sum_{f,f'} J_{f,f'}^d d_f^\dagger d_{f'} + \sum_f J_{f,0,f,1}^c (c_{f,0}^\dagger c_{f,1} + h.c.) + J_{f,0,f-1,\delta-1}^c (c_{f,0}^\dagger c_{f-1,\delta-1} + h.c.) \quad (20)$$

Using such a generator, one can employ the same ansatz as above, but the transformation now results in a novel fixed point Hamiltonian describing transport between uncoupled sites and conserved charges on coupled and dirty sites ($n_{f,r=0}^c$ and n_f^d respectively). In addition, the new generator produces a next-nearest neighbor hopping across the coupled site (i.e. $J_{f,r=\delta-1,f'=f+1,r=1}$). In the proceeding section we derive this hopping rate as $\frac{1}{\tau_n} = [J^c(l=0)]^2 / \bar{h}^c(l=0)$, which in the limit of strong inter-chain coupling, Δ^I , is smaller than the other timescales in the system. In this limit, relaxation occurs in two steps: first, on times scales shorter than τ_n , transport is blocked by the coupled sites, and second, on times scales longer than τ_n , charge is allowed to diffuse across the coupled sites. In the first step, when $\tau \lesssim \tau_n$, the system relaxes to a state in which the charge on the bunches of uncoupled sites, $N_f = \sum_{r=1}^{\delta} n_{f,r}^c$, is conserved. While on longer times, charge on the uncoupled sites can fully relax via unconstrained transport. In the following two sections, we further investigate this novel behavior by first, in section 6.1, deriving the time, τ_n , separating the two relaxation steps, and second, in section 6.2, investigating and deriving the Hamiltonian that governs short time relaxation.

6.1. Separation of Time Scales

To derive an estimate of the next-nearest neighbor hopping rate, we first assume $\Delta \ll W$. This guarantees that the flow of the dirty chain reaches a steady state before there are significant changes in the clean one. We can then treat the clean chain as a single chain with an effective field $\bar{h}_{f,r}$. We write the new generator as

$$\eta' = \sum_f \eta_f \quad (21)$$

where

$$\eta_f = -J\bar{h}_{f,0}(c_{f-1,\delta-1}^\dagger c_{f,0} - h.c) + J\bar{h}_{f,0}(c_{f,0}^\dagger c_{f,1} - h.c), \quad (22)$$

with J the strength of the hopping on to the coupled site. The first term in η_f will suppress hopping between the coupled site and its left neighbor, while the second term will enforce the

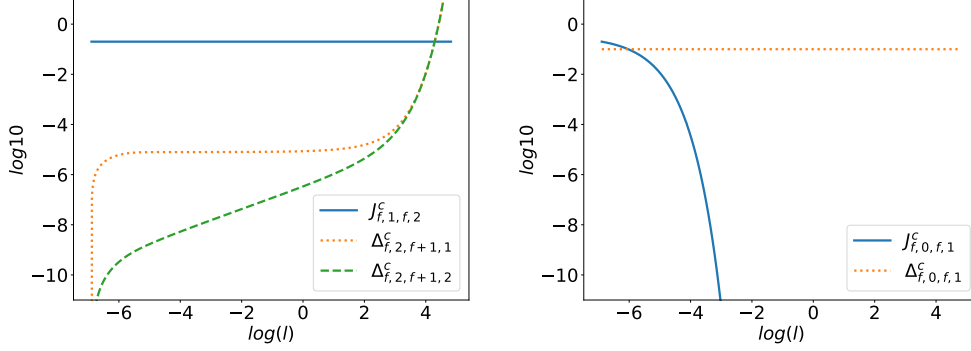


Figure 7: The flow of J_{ij}^c and Δ_{ij}^c , for the geometry depicted in Fig. 6. The left panel shows the flow of couplings on the clean-chain sites that are not coupled to the dirty chain. It shows an unsuppressed hopping and diverging density-density coupling at long flow time l . The right panel shows the flow of couplings on the clean chain sites that involve a site coupled to the dirty chain. It shows that the hopping onto the coupled site, $r = 0$ (for any f), are suppressed and the density-density coupling involving a coupled site, remains constant instead. This calculation has been performed using an unmodified generator $\eta = [H_0, V]$; in order to remove the divergences in $\Delta_{f,r,f',r'}^c$, we modify the generator to $\eta = [H_0, V']$, with V' given in Eq. 20.

same on the right neighbor. Since $[\eta_f, \eta_{f'}] = 0$ for $\delta > 2$, we can focus on a single coupled site and its neighbor.

We will label the coupled site with 0 and its left and right neighbor sites with -1 and $+1$. The hopping and effective field couplings will then flow as

$$\begin{aligned}
\frac{d\bar{h}_{\pm 1}}{dl} &= -2J^2\bar{h}_0, \\
\frac{d\bar{h}_0}{dl} &= 2J^2\bar{h}_{+1} + 2J^2\bar{h}_{-1}, \\
\frac{dJ}{dl} &= -J\bar{h}_0^2, \\
\frac{dJ_2}{dl} &= 2J^2\bar{h}_0,
\end{aligned} \tag{23}$$

where J_2 is the magnitude of the next-nearest neighbor hopping, $J_2(l) = J_{f,r=\delta-1,f'=f+1,r=1}(l)$.

The flow of these couplings do not depend on the flow of the density-density coupling and can thus be solved independently. We use the assumption that $J \ll \bar{h}$ and note that the flow of J is much faster than the flow of the other couplings. Thus, assuming \bar{h} constant, we can approximate the flow of $J(l)$ as

$$J(l) = J(l=0)e^{-\bar{h}_0^2 l}. \tag{24}$$

Approximating \bar{h}_0 as constant, we find

$$J_2(l) = -\frac{J^2}{\bar{h}_0}(1 - e^{-2\bar{h}_0^2 l}). \tag{25}$$

Thus, $\tau_n = \frac{\bar{h}_0}{J^2}$ is the characteristic time when relaxation crosses over to full transport and eventually to thermalization. A meaningful separation of time scales therefore requires $\bar{h}_0 \gg J^2$.

In the following section we will discuss the form of the effective Hamiltonian describing the first stage of relaxation.

6.2. Effective Hamiltonian at intermediate times: $\tau \lesssim \tau_n$

As discussed above, relaxation in the novel geometry with large inter-chain coupling, occurs in two stages: first, during intermediate times, the model relaxes to a state in which the clean-charge distribution on the uncoupled clusters is approximately conserved, while, on longer times, the clean-charge relaxes to a homogeneous distribution. The Hamiltonian describing the first relaxation process is obtained by dropping the next nearest neighbor hoppings from the Hamiltonian, $H(l \rightarrow \infty)$. This Hamiltonian, has 3 types of conserved charges as depicted in Fig. 6: the first type, n_k^d , are the conserved charges on the dirty chain, the second type $n_{f,r=0}^c$ are the conserved charge on the coupled site and $N_f = \sum_{r=1}^{\delta} n_{f,r}^c$ is the total conserved charge on an uncoupled cluster. For $\delta > 2$ these charges do not determine the dynamics of the charge distribution within an uncoupled cluster, and we must consider the interplay between the intra-cluster tunneling and inter-cluster density-density coupling.

There are two possibilities for such interplay: the density-density coupling between two neighboring sets of uncoupled sites is smaller than J_2 , or it is larger:

- In the first case, the density-density coupling can be accurately dropped from the intermediate time effective Hamiltonian. This leads to each set of uncoupled sites, labeled by f , evolving completely independently on intermediate times. The dynamics can be described as the evolution of an effective spin, $\vec{L}_f = \{L_x, L_y, L_z\}$, of size

$$|\vec{L}_f| = \frac{1}{2} \left(\frac{\delta - 1}{N_f} \right) + \frac{1}{2}. \quad (26)$$

The local map between the N_f fermions on $\delta - 1$ sites and the spin can be performed by identifying the basis states labeled by the eigenvalues of $n_{f,r \neq 0}^c$ with the basis states labeled by the eigenvalues of L_f^z . Operators that are polynomial in the densities will then be mapped to operators that are polynomial in L_z . The remaining terms in the Hamiltonian describe tunneling within a set of uncoupled sites with all the same f . They describe transition between the L_f^z basis states and are thus described by polynomials in L_f^x and L_f^y .

- In the second case, when the density-density interaction between the uncoupled cluster is relevant, the local emergent spins will be coupled. Since the hopping operators at a site f commute with those at a site f' , a Jordan-Wigner string is not required to correctly reproduce spin statistics, and the coupled Hamiltonian can be written as:

$$H(\{\bar{n}_f^d\}, \{\bar{n}_{f,r=0}^c\}, \{\bar{N}_f\}) = \sum_{ff'} F(L_f^z, L_{f'}^z) + \sum_f R_f(L_f^x, L_f^z, L_f^y), \quad (27)$$

where the function F depends on the intra-chain coupling, Δ^c , and the function R depends on $h_k^c, J_{ij}^c, \Delta_{ij}^I$, and Δ_{ij}^c . In general, if the dirty chain or coupled sites have a disordered distribution of charges, the local operators, R_f , in the Hamiltonian will be disordered too.

The issue of whether the system is fully localized on intermediate times, will then depend on any integrability present in this intermediate time Hamiltonian, or on the impact of disorder on R_f .

In the first case, the intermediate time Hamiltonian can be diagonalized by independently diagonalizing the Hamiltonian of effective spins L_f . In the second case, when the spins are coupled, further analysis is required to explore the dynamics at intermediate times and will be the subject of Sec. 6.4.

6.3. Density-Density interactions between uncoupled clusters

To determine if the effective spins \vec{L}_f are coupled or not, we compute the magnitude of the density-density interaction between two uncoupled clusters. We focus again on one coupled site, labeled by $r = 0$, and its neighboring sites, labeled by $r = \pm 1$ (for any f). The flow equation equations for the density-density couplings then becomes

$$\begin{aligned}\frac{d\Delta_{-1,1}^c}{dl} &= 2J^2(\Delta_{-1,1}^c - \Delta_{0,1}^c) + 2J^2(\Delta_{-1,1}^c - \Delta_{0,-1}^c), \\ \frac{d\Delta_{0,1}^c}{dl} &= -2J^2(\Delta_{-1,1}^c - \Delta_{0,1}^c), \\ \frac{d\Delta_{-1,0}^c}{dl} &= -2J^2(\Delta_{-1,1}^c - \Delta_{0,-1}^c).\end{aligned}\tag{28}$$

These coupled differential equations describe a rotation in a three-dimensional space at an instantaneous rate $2J(l)^2$. Given that $\Delta_{-1,1}^c(l=0) = 0$, the system (28) can be solved and yields

$$\Delta_{-1,1}^c(l) = \Delta_{0,1}^c(l=0) \left[1 - e^{\int_0^l dt' 2J^2(t')} \right],\tag{29}$$

where:

$$\int_0^l dt' 2J^2(t') = \frac{J^2(l=0)}{\hbar_0^2(l=0)} (1 - e^{-2\hbar_0^2 l}).\tag{30}$$

Therefore, the amplitude of the rotation in such three-dimensional parameter space is small in J^2/\hbar_0^2 .

We are now in place to discuss which of the two possibilities discussed in the previous section is realized. If $J_2(l=\infty) \ll \Delta_{-1,1}(l=\infty)$, then an interacting Hamiltonian describes the intermediate time dynamics while, if the inequality is not satisfied, a non-interacting spin chain will describes the intermediate time dynamics. Given the assumption $J \ll h$, this inequality simplifies to $h \ll \Delta$. Thus, for the approximation made in ansatz Hamiltonian above, we must choose $h > \Delta$ and conclude that the intermediate time Hamiltonian describes a set of independently evolving spins.

Alternatively, we could assume the bare Hamiltonian has a next-nearest neighbor coupling of the order $\Delta_{-1,1}(l=0) \approx \Delta_{0,1} < h$. In this case the rotation in Δ_{ij}^c space, described by Eq. 28, would still be of a small angle, but away from an initial vector with $\Delta_{-1,1}(l=0)$ already greater than $J_2(l=\infty)$. Intermediate time dynamics would then be described by a set of coupled emergent spins of size $|\vec{L}_f|$.

6.4. Explicit form of the Hamiltonian for $\delta = 3$

As an example, we now can consider the $\delta = 3$ case in which there are two uncoupled sites for each dirty site f , and discuss the effective Hamiltonian governing the intermediate time dynamics. The local Hilbert space for these two sites is 4 dimensional and the basis vectors can be labeled by the different ways in which 2 sites may be occupied with particles (the label '1' indicates an occupied site)

$$\{|00\rangle, |01\rangle, |10\rangle, |11\rangle\}, \quad (31)$$

The local Hamiltonian on these sites reflects the block diagonal structure enforced by the conserved charges:

$$\begin{bmatrix} 0 & 0 & 0 & 0 \\ 0 & \tilde{\Delta}^L & J_{f2,f1}^c(l) & 0 \\ 0 & J_{f1,f2}^c(l) & \tilde{\Delta}^R & 0 \\ 0 & 0 & 0 & \tilde{\Delta}^{R+L} \end{bmatrix}, \quad (32)$$

where $\tilde{\Delta}^L, \tilde{\Delta}^R$, and $\tilde{\Delta}^{R+L}$ are functions linear in the operators n_i^d and $n_{f' \neq f}^c$ and depend on the intra and inter-chain couplings, and fields h^c , at the flow time $l = \infty$. For $\delta = 3$ the conserved charge N_f has eigenvalues 0, 1, and 2 that correspond to the three blocks in Eq. 32. This block structure can be represented by two trivial spin-zero subspaces and one spin-half subspace.

We consider the case that $N_f = 1$ for each f , so that the local Hilbert space for the block of interest will be spin-half. The mapping to spin-halves can be performed via

$$\begin{aligned} L_f^z &= \frac{\hat{n}_{f,1} - \hat{n}_{f,2}}{2} \\ L_f^x &= \frac{c_{f,1}^\dagger c_{f,2} + h.c.}{2}, \end{aligned} \quad (33)$$

and the constraint $\frac{1}{2} = \frac{\hat{n}_{f,1} + \hat{n}_{f,2}}{2}$.

We write down the Hamiltonian at the flow time $l = \infty$ as follows:

$$\begin{aligned} H &= \sum_f H_f + \sum_{f,f'} \sum_{r,r'=1,2} \Delta_{f,r,f',r'}^c n_{f,r}^c n_{f',r'}^c \\ H_f &= \sum_i \xi_{f,i} n_{f,i} + J_f^u(l) [c_{f,1}^\dagger c_{f,2} + c_{f,2}^\dagger c_{f,1}] \\ &\quad + \Delta_{f,1,f,2}^c n_{f,2}^c n_{f,1}^c, \end{aligned} \quad (34)$$

where $\xi_{f,i}$ is an effective field that depends on the bare fields at flow time l , the couplings Δ_{ij}^c and Δ_{ij}^I , and the eigenvalues of the conserved charges, \bar{n}_f^d and $\bar{n}_{f,r=0}^c$:

$$\xi_{f,i} = \bar{h}_{f,i}^c(l) + \sum_f \Delta_{f,i,f'}^I(l) \bar{n}_{f'}^d + \sum_f \Delta_{f,i,f',0}^c(l) \bar{n}_{f',0}^c.$$

Applying the mapping (33) we get the spin Hamiltonian:

$$H = \sum_f h_f^z L_f^z + h_f^x L_f^x + \sum_{ff'} \Omega_{f,f'} L_f^z L_{f'}^z + C \quad (35)$$

with

$$\begin{aligned}
h_f^x &= 2J_f^{un}(l) \\
h_f^z &= \xi_{f,1} - \xi_{f,2} \\
\Omega_{f,f'} &= \Delta_{f,1,f',1}^C + \Delta_{f,2,f',2}^C - \Delta_{f,1,f',2}^C - \Delta_{f,2,f',1}^C.
\end{aligned} \tag{36}$$

Here, we explicitly see how the spins are coupled by the next-nearest neighbor density-density couplings. Thus, if the local spins are coupled at a strength less than the next-nearest neighbor hopping, $|\Omega_{f,f'}| < J_2$, the intermediate time dynamics describes independent spins rotating around an axis in the $x - z$ plane. While, if $|\Omega_{f,f'}| > J_2$, we have to consider the interacting spin problem to understand the intermediate time dynamics.

If there is no disorder in the dirty and coupled site charge distributions, the z component of the local field, h_f^z will be null and the translationally-invariant emergent spin-model will be a transverse field Ising model. This Hamiltonian is integrable via the Jordan-Wigner transformation:

$$\begin{aligned}
L_f^x &\rightarrow n_f^a - 1/2 \\
L_f^z L_{f+1}^z &\rightarrow (a_f^\dagger - a_f)(a_{f+1} + a_{f+1}^\dagger),
\end{aligned} \tag{37}$$

which produces an exactly solvable single particle Hamiltonian in Jordan-Wigner fermions. Taking $\Omega_{f,f'} = \Omega \delta_{f',f+1}$, this single particle Hamiltonian is given as

$$\sum_f h^x n_f^a + \Omega(a_f^\dagger a_{f+1} + h.c.) + \Omega(a_f^\dagger a_{f+1}^\dagger + h.c.), \tag{38}$$

which can be brought in diagonal form $\sum_q \omega_q n_q$ in momentum space via a Bogolyubov rotation, where n_q is the occupation of the mode q and $\omega_q = \sqrt{1 + 2\frac{\Omega}{h} \cos(q) + \frac{\Omega^2}{h^2}}$. We therefore, in addition to the local conserved charges, $n_{f,0}^c$, n_f^d , N_F , have the conserved momentum space modes n_q . The non ergodic behavior during intermediate times after the initial relaxation period and before τ_n will display a mixture of local conserved charges, and extended conserved charges, n_q .

If there is disorder in the dirty and coupled site charge distributions, the z -components of the local field, h_z , given in Eq. 36 will be finite. The Jordan-Wigner transformation of L_f^z will introduce a many body operator via the Jordan-Wigner string, $L_f^z = a_f^\dagger e^{i\pi \sum_f N_f} + h.c.$, and the new fermion Hamiltonian will no longer be diagonalizable via a single particle transformation. In this case, n_q will no longer be conserved and, if h^z is weak compared to the transverse field h_f^x , only the local conserved charges, $n_{f,0}^c$, n_f^d , and N_F , will survive after the first relaxation period. If the disorder field, h_f^z , dominates over the transverse field, h_f^x , the effective Hamiltonian, Eq. 35, will many body localize and develop a set of local conserved charges L_f^z . We have confirmed these expectations via exact diagonalization of the intermediate time Hamiltonian and by studying the level spacing statistics for $N_s = 8$ and $\delta N_s = 24$ ($\delta = 3$).

7. Conclusions

A natural direction we are currently scrutinizing consists in extending the FE method to capture physics akin to the one reported in the experiment of Ref. [63]. However, in order to

have a quantitative understanding of the delocalizing impact of the clean environment on the disordered chain, one should assume that the clean chain is delocalized, and therefore extend the ansatz employed here to treat Hamiltonian diagonal in momentum space. It could also be of interest to employ the FE method to study a broader variety of MBL proximity effects. An appealing direction consists in studying a point-like, local coupling, between an MBL segment of interacting, disordered fermions and a clean one. This would pave way to understand the effect of the 'intrusion' of the localized system into the clean one, or viceversa, explore how an MBL system can act as an 'insulator' with respect to the clean segment. Analysis in this direction is ongoing [65].

Acknowledgments

S. P. K. and J. M. are indebted with S. J. Thomson and M. Schiro for helpful and clarifying discussions and exchanges on the flow equation method for MBL systems. We thank I. Bloch for inspiring discussions. JM is supported by the European Union's Horizon 2020 research and innovation programme under the Marie Skłodowska-Curie grant agreement No 745608 (QUAKE4PRELIMAT). This research was supported in part by the National Science Foundation under Grant No. NSF PHY-1748958.

This work is based upon work supported in part (RN, JM) by the Air Force office of Scientific Research under award number FA 9550-17-1-0183.

S. P. K. acknowledges financial support from the UC Office of the President through the UC Laboratory Fees Research Program, Award Number LGF-17- 476883

Los Alamos National Laboratory is managed by Triad National Security, LLC, for the National Nuclear Security Administration of the U.S. Department of Energy under Contract No. 89233218CNA000001

References

References

- [1] I. Bloch, J. Dalibard, W. Zwerger, [Many-body physics with ultracold gases](https://doi.org/10.1103/RevModPhys.80.885), Rev. Mod. Phys. 80 (2008) 885–964. doi:10.1103/RevModPhys.80.885. URL <https://link.aps.org/doi/10.1103/RevModPhys.80.885>
- [2] F. H. L. Essler, M. Fagotti, [Quench dynamics and relaxation in isolated integrable quantum spin chains](https://arxiv.org/abs/1606.06402), J. Stat. Mech. 2016 (6) (2016) 064002. URL <http://stacks.iop.org/1742-5468/2016/i=6/a=064002>
- [3] P. Calabrese, J. Cardy, Quantum quenches in 1+1 dimensional conformal field theories, J. Stat. Mech. 064003.
- [4] C. J. Turner, A. A. Michailidis, D. A. Abanin, M. Serbyn, Z. Papic, Nature Physics, 14, 7, 745-749.
- [5] R. Nandkishore, D. A. Huse, [Many-body localization and thermalization in quantum statistical mechanics](https://doi.org/10.1146/annurev-conmatphys-031214-014726), Annual Review of Condensed Matter Physics 6 (1) (2015) 15–38. doi:10.1146/annurev-conmatphys-031214-014726. URL <http://dx.doi.org/10.1146/annurev-conmatphys-031214-014726>
- [6] D. Abanin, E. Altman, I. Bloch, M. Serbyn, arXiv:1804.11065.
- [7] B. L. Altshuler, Y. Gefen, A. Kamenev, L. S. Levitov, [Quasiparticle lifetime in a finite system: A non-perturbative approach](https://doi.org/10.1103/PhysRevLett.78.2803), Phys. Rev. Lett. 78 (1997) 2803–2806. doi:10.1103/PhysRevLett.78.2803. URL <https://link.aps.org/doi/10.1103/PhysRevLett.78.2803>
- [8] D. Basko, I. Aleiner, B. Altshuler, [Metal-insulator transition in a weakly interacting many-electron system with localized single-particle states](https://doi.org/10.1016/j.aop.2005.11.014), Annals of Physics 321 (5) (2006) 1126 – 1205. doi:10.1016/j.aop.2005.11.014. URL <http://www.sciencedirect.com/science/article/pii/S0003491605002630>

- [9] I. V. Gornyi, A. D. Mirlin, D. G. Polyakov, **Electron transport in a disordered luttinger liquid**, Phys. Rev. B 75 (2007) 085421. doi:10.1103/PhysRevB.75.085421.
URL <https://link.aps.org/doi/10.1103/PhysRevB.75.085421>
- [10] A. Pal, D. A. Huse, **Many-body localization phase transition**, Phys. Rev. B 82 (2010) 174411. doi:10.1103/PhysRevB.82.174411.
URL <http://link.aps.org/doi/10.1103/PhysRevB.82.174411>
- [11] M. Znidaric, T. Prosen, P. Prelovsek, **Many-body localization in the heisenberg xxz magnet in a random field**, Phys. Rev. B 77 (2008) 064426. doi:10.1103/PhysRevB.77.064426.
URL <http://link.aps.org/doi/10.1103/PhysRevB.77.064426>
- [12] V. Oganesyan, D. A. Huse, **Localization of interacting fermions at high temperature**, Phys. Rev. B 75 (2007) 155111. doi:10.1103/PhysRevB.75.155111.
URL <http://link.aps.org/doi/10.1103/PhysRevB.75.155111>
- [13] V. Khemani, R. Nandkishore, S. L. Sondhi, **Nonlocal adiabatic response of a localized system to local manipulations**, Nat Phys 11 (7) (2015) 560–565.
URL <http://dx.doi.org/10.1038/nphys3344>
- [14] S. Gopalakrishnan, M. Müller, V. Khemani, M. Knap, E. Demler, D. A. Huse, **Low-frequency conductivity in many-body localized systems**, Phys. Rev. B 92 (2015) 104202. doi:10.1103/PhysRevB.92.104202.
URL <http://link.aps.org/doi/10.1103/PhysRevB.92.104202>
- [15] J. H. Bardarson, F. Pollmann, J. E. Moore, **Unbounded growth of entanglement in models of many-body localization**, Phys. Rev. Lett. 109 (2012) 017202. doi:10.1103/PhysRevLett.109.017202.
URL <https://link.aps.org/doi/10.1103/PhysRevLett.109.017202>
- [16] S. D. Geraedts, R. Nandkishore, N. Regnault, **Many-body localization and thermalization: Insights from the entanglement spectrum**, Phys. Rev. B 93 (2016) 174202. doi:10.1103/PhysRevB.93.174202.
URL <https://link.aps.org/doi/10.1103/PhysRevB.93.174202>
- [17] V. Khemani, S. P. Lim, D. N. Sheng, D. A. Huse, **Critical properties of the many-body localization transition**, Phys. Rev. X 7 (2017) 021013. doi:10.1103/PhysRevX.7.021013.
URL <https://link.aps.org/doi/10.1103/PhysRevX.7.021013>
- [18] Z.-C. Yang, A. Hamma, S. M. Giampaolo, E. R. Mucciolo, C. Chamon, **Entanglement Complexity in Quantum Many-Body Dynamics, Thermalization and Localization**, ArXiv e-prints [arXiv:1703.03420](https://arxiv.org/abs/1703.03420).
- [19] S. D. Geraedts, N. Regnault, R. M. Nandkishore, **Characterizing the many-body localization transition using the entanglement spectrum**, New Journal of Physics 19 (11) (2017) 113021.
URL <http://stacks.iop.org/1367-2630/19/i=11/a=113021>
- [20] D. A. Huse, R. Nandkishore, V. Oganesyan, A. Pal, S. L. Sondhi, **Localization-protected quantum order**, Phys. Rev. B 88 (2013) 014206. doi:10.1103/PhysRevB.88.014206.
URL <http://link.aps.org/doi/10.1103/PhysRevB.88.014206>
- [21] D. Pekker, G. Refael, E. Altman, E. Demler, V. Oganesyan, **Hilbert-glass transition: New universality of temperature-tuned many-body dynamical quantum criticality**, Phys. Rev. X 4 (2014) 011052. doi:10.1103/PhysRevX.4.011052.
URL <http://link.aps.org/doi/10.1103/PhysRevX.4.011052>
- [22] R. Vosk, E. Altman, **Dynamical quantum phase transitions in random spin chains**, Phys. Rev. Lett. 112 (2014) 217204. doi:10.1103/PhysRevLett.112.217204.
URL <http://link.aps.org/doi/10.1103/PhysRevLett.112.217204>
- [23] R. Vosk, E. Altman, **Many-body localization in one dimension as a dynamical renormalization group fixed point**, Phys. Rev. Lett. 110 (2013) 067204. doi:10.1103/PhysRevLett.110.067204.
URL <https://link.aps.org/doi/10.1103/PhysRevLett.110.067204>
- [24] M. Serbyn, Z. Papić, D. A. Abanin, **Local conservation laws and the structure of the many-body localized states**, Phys. Rev. Lett. 111 (2013) 127201. doi:10.1103/PhysRevLett.111.127201.
URL link.aps.org/doi/10.1103/PhysRevLett.111.127201
- [25] D. A. Huse, R. Nandkishore, V. Oganesyan, **Phenomenology of fully many-body-localized systems**, Phys. Rev. B 90 (2014) 174202. doi:10.1103/PhysRevB.90.174202.
URL <http://link.aps.org/doi/10.1103/PhysRevB.90.174202>
- [26] V. Ros, M. Müller, A. Scardicchio, **Integrals of motion in the many-body localized phase**, Nuclear Physics B 891 (2015) 420–465. doi:<http://dx.doi.org/10.1016/j.nuclphysb.2014.12.014>.
URL <http://www.sciencedirect.com/science/article/pii/S0550321314003836>
- [27] A. Chandran, A. Pal, C. R. Laumann, A. Scardicchio, ArXiv e-prints: 1605.00655.
- [28] S. D. Geraedts, R. N. Bhatt, R. Nandkishore, **Emergent local integrals of motion without a complete set of localized eigenstates**, Phys. Rev. B 95 (2017) 064204. doi:10.1103/PhysRevB.95.064204.
URL <http://link.aps.org/doi/10.1103/PhysRevB.95.064204>
- [29] S. A. Parameswaran, S. Gopalakrishnan, **Non-Fermi glasses: fractionalizing electrons at finite energy density**,

- ArXiv e-prints [arXiv:1608.00981](https://arxiv.org/abs/1608.00981).
- [30] J. Z. Imbrie, **Diagonalization and many-body localization for a disordered quantum spin chain**, Phys. Rev. Lett. 117 (2016) 027201. doi:10.1103/PhysRevLett.117.027201. URL <https://link.aps.org/doi/10.1103/PhysRevLett.117.027201>
- [31] M. Schreiber, S. S. Hodgman, P. Bordia, H. P. Lüschen, M. H. Fischer, R. Vosk, E. Altman, U. Schneider, I. Bloch, Observation of many-body localization of interacting fermions in a quasi-random optical lattice, Science 349 (6250) (2015) 842–845. doi:10.1126/science.aaa7432.
- [32] P. Bordia, H. P. Lüschen, S. S. Hodgman, M. Schreiber, I. Bloch, U. Schneider, **Coupling identical one-dimensional many-body localized systems**, Phys. Rev. Lett. 116 (2016) 140401. doi:10.1103/PhysRevLett.116.140401. URL <https://link.aps.org/doi/10.1103/PhysRevLett.116.140401>
- [33] J. Choi, S. Hild, J. Zeiher, P. Schauss, A. Rubio-Abadal, T. Yefsah, V. Khemani, D. A. Huse, I. Bloch, C. Gross, Exploring the many-body localization transition in two dimensions, Science 352 (6293) (2016) 1547–1552. doi:10.1126/science.aaf8834.
- [34] M. Rispoli, A. Lukin, R. Schittko, S. Kim, M. E. Tai, J. Leonard, M. Greiner, arXiv:1812.06959.
- [35] P. Roushan, C. Neill, J. Tangpanitanon, V. M. Bastidas, A. Megrant, R. Barends, Y. Chen, Z. Chen, B. Chiaro, A. Dunsworth, et al., Science 358, 1175–1179.
- [36] R. Nandkishore, S. Gopalakrishnan, D. A. Huse, **Spectral features of a many-body-localized system weakly coupled to a bath**, Phys. Rev. B 90 (2014) 064203. doi:10.1103/PhysRevB.90.064203. URL <https://link.aps.org/doi/10.1103/PhysRevB.90.064203>
- [37] R. Nandkishore, S. Gopalakrishnan, **Many body localized systems weakly coupled to baths**, Annalen der Physik (2016) 1521–3889 doi:10.1002/andp.201600181. URL <http://dx.doi.org/10.1002/andp.201600181>
- [38] S. Gopalakrishnan, R. Nandkishore, **Mean-field theory of nearly many-body localized metals**, Phys. Rev. B 90 (2014) 224203. doi:10.1103/PhysRevB.90.224203. URL <https://link.aps.org/doi/10.1103/PhysRevB.90.224203>
- [39] S. Banerjee, E. Altman, **Variable-range hopping through marginally localized phonons**, Phys. Rev. Lett. 116 (2016) 116601. doi:10.1103/PhysRevLett.116.116601. URL <https://link.aps.org/doi/10.1103/PhysRevLett.116.116601>
- [40] M. H. Fischer, M. Maksymenko, E. Altman, **Dynamics of a many-body-localized system coupled to a bath**, Phys. Rev. Lett. 116 (2016) 160401. doi:10.1103/PhysRevLett.116.160401. URL <https://link.aps.org/doi/10.1103/PhysRevLett.116.160401>
- [41] E. Levi, M. Heyl, I. Lesanovsky, J. P. Garrahan, **Robustness of many-body localization in the presence of dissipation**, Phys. Rev. Lett. 116 (2016) 237203. doi:10.1103/PhysRevLett.116.237203. URL <https://link.aps.org/doi/10.1103/PhysRevLett.116.237203>
- [42] M. Medvedyeva, T. Prosen, M. Znidaric, **Influence of dephasing on many-body localization**, Phys. Rev. B 93 (2016) 094205. doi:10.1103/PhysRevB.93.094205. URL <https://link.aps.org/doi/10.1103/PhysRevB.93.094205>
- [43] W. De Roeck, F. Huveneers, arXiv 1608.01815.
- [44] D. J. Luitz, F. Huveneers, W. De Roeck, **How a small quantum bath can thermalize long localized chains**, Phys. Rev. Lett. 119 (2017) 150602. doi:10.1103/PhysRevLett.119.150602. URL <https://link.aps.org/doi/10.1103/PhysRevLett.119.150602>
- [45] P. Ponte, C. Laumann, D. Huse, A. Chandran, Thermal inclusions: how one spin can destroy a many-body localized phase, Philosophical Transactions A.
- [46] S. Lorenzo, T. Apollaro, G. M. Palma, R. Nandkishore, A. Silva, J. Marino, **Remnants of anderson localization in prethermalization induced by white noise**, Phys. Rev. B 98 (2018) 054302. doi:10.1103/PhysRevB.98.054302. URL <https://link.aps.org/doi/10.1103/PhysRevB.98.054302>
- [47] H. P. Lüschen, P. Bordia, S. S. Hodgman, M. Schreiber, S. Sarkar, A. J. Daley, M. H. Fischer, E. Altman, I. Bloch, U. Schneider, **Signatures of many-body localization in a controlled open quantum system**, Phys. Rev. X 7 (2017) 011034. doi:10.1103/PhysRevX.7.011034. URL <https://link.aps.org/doi/10.1103/PhysRevX.7.011034>
- [48] R. Nandkishore, **Many-body localization proximity effect**, Phys. Rev. B 92 (2015) 245141. doi:10.1103/PhysRevB.92.245141. URL <https://link.aps.org/doi/10.1103/PhysRevB.92.245141>
- [49] K. Hyatt, J. R. Garrison, A. C. Potter, B. Bauer, Many-body localization in the presence of a small bath, Physical Review B 95. doi:10.1103/PhysRevB.95.035132.
- [50] J. Marino, R. M. Nandkishore, **Many-body localization proximity effects in platforms of coupled spins and bosons**, Phys. Rev. B 97 (2018) 054201. doi:10.1103/PhysRevB.97.054201.

- URL <https://link.aps.org/doi/10.1103/PhysRevB.97.054201>
- [51] S. Kehrein, *The flow equation approach to many-particle systems*, Springer, 2007.
- [52] R. Vosk, D. A. Huse, E. Altman, **Theory of the many-body localization transition in one-dimensional systems**, *Phys. Rev. X* 5 (2015) 031032. doi:10.1103/PhysRevX.5.031032.
URL <https://link.aps.org/doi/10.1103/PhysRevX.5.031032>
- [53] A. C. Potter, R. Vasseur, S. A. Parameswaran, **Universal properties of many-body delocalization transitions**, *Phys. Rev. X* 5 (2015) 031033. doi:10.1103/PhysRevX.5.031033.
URL <https://link.aps.org/doi/10.1103/PhysRevX.5.031033>
- [54] P. T. Dumitrescu, R. Vasseur, A. C. Potter, **Scaling theory of entanglement at the many-body localization transition**, *Phys. Rev. Lett.* 119 (2017) 110604. doi:10.1103/PhysRevLett.119.110604.
URL <https://link.aps.org/doi/10.1103/PhysRevLett.119.110604>
- [55] T. Thiery, F. Huveneers, M. Müller, W. De Roeck, **Many-body delocalization as a quantum avalanche**, *Phys. Rev. Lett.* 121 (2018) 140601. doi:10.1103/PhysRevLett.121.140601.
URL <https://link.aps.org/doi/10.1103/PhysRevLett.121.140601>
- [56] S.-X. Zhang, H. Yao, **Universal properties of many-body localization transitions in quasiperiodic systems**, *Phys. Rev. Lett.* 121 (2018) 206601. doi:10.1103/PhysRevLett.121.206601.
URL <https://link.aps.org/doi/10.1103/PhysRevLett.121.206601>
- [57] A. Goremykina, R. Vasseur, M. Serbyn, **Analytically solvable renormalization group for the many-body localization transition**, *Phys. Rev. Lett.* 122 (2019) 040601. doi:10.1103/PhysRevLett.122.040601.
URL <https://link.aps.org/doi/10.1103/PhysRevLett.122.040601>
- [58] F. Wegner, Flow-equations for hamiltonians, *Annalen der Physik* 506 (2) (1994) 77–91.
- [59] D. Pekker, B. K. Clark, V. Oganesyan, G. Refael, Fixed points of wegner-wilson flows and many-body localization, *Phys. Rev. Lett.* 119 (2017) 075701. doi:10.1103/PhysRevLett.119.075701.
- [60] S. Thomson, M. Schiro, arXiv:cond-mat (2018) Phys. Rev. B 97, 060201.
- [61] C. Monthus, Flow towards diagonalization for many-body-localization models: adaptation of the toda matrix differential flow to random quantum spin chains, *Journal of Physics A: Mathematical and Theoretical* 49 (30) (2016) 305002.
- [62] V. K. Varma, A. Raj, S. Gopalakrishnan, V. Oganesyan, D. Pekker, **Length scales in the many-body localized phase and their spectral signatures**, arXiv:1901.02902 [cond-mat, physics:quant-ph]ArXiv: 1901.02902.
URL <http://arxiv.org/abs/1901.02902>
- [63] A. Rubio-Abadal, J. Choi, J. Zeiher, S. Hollerith, J. Rui, I. Bloch, C. Gross, arXiv:1805.00056.
- [64] J. Stein, **Flow equations and the strong-coupling expansion for the hubbard model**, *Journal of Statistical Physics* 88 (1) (1997) 487–511. doi:10.1007/BF02508481.
URL <https://doi.org/10.1007/BF02508481>
- [65] S. Kelly, et al., in preparation.

Appendix A. Notation

We define the onsite fields before Wick ordering as $h_k^{c(d)}$, and after Wick ordering, the effective fields are defined with a bar: $\bar{h}_k^{c(d)}$. We define the couplings with unaccented variables with subscripts indexing sites: $\Delta_{ij}^I, \Delta_{ij}^{c(d)}, J_{ij}^{c(d)}$. The dependence on the scale l of the flow equations is often made implicit in expressions: $\Delta_{ij}^I(l) \rightarrow \Delta_{ij}^I$. For Δ_{ij}^I the first index i labels the clean chain sites and the second the dirty chain sites. The spatial dependence of the couplings defines geometry and the magnitude is set by the parameters $\Delta^{I(c,d)}, J^{c(d)}$. In addition to these parameters, the dirty chain fields are randomly selected from a box distribution, $[-W, W]$, and the Wick ordered reference state is set by: $\langle n^d \rangle = \frac{1}{N_s} \sum_k \langle n_k^d \rangle$ and temperature Θ , where $\langle n_k^d \rangle = \text{Tr}[\rho n_k^d]$

We work with a set of unaccented operators: $U, H, H_0, V, H^c, H^d, H^I, \eta_h, \eta_\Delta, \eta_I, c_k, d_k, n_k^c, n_k^d$

and $\vec{L}_f = \{L_f^x, L_f^y, L_f^z\}$. We also define a set of operators accented with a hat as:

$$\begin{aligned}
\hat{J}^c &= \sum_{ij} J_{ij}^c : c_i^\dagger c_j : \\
\hat{J}^d &= \sum_{ij} J_{ij}^d : d_i^\dagger d_j : \\
\hat{\Delta}^c &= \sum_{ij} \Delta_{ij}^c : n_i^c n_j^c : \\
\hat{\Delta}^d &= \sum_{ij} \Delta_{ij}^d : n_i^d n_j^d : \\
\hat{\Delta}^I &= \sum_{ij} \Delta_{ij}^I : n_i^c n_j^d : \\
\hat{h}^c &= \sum_k \bar{h}_k^c : n_k^c : \\
\hat{h}^d &= \sum_k \bar{h}_k^d : n_k^c : .
\end{aligned} \tag{A.1}$$

Finally, we also defined a symmetry operation, $C \leftrightarrow D$, that swaps the superscripts c and d of the couplings and operators and swaps the site indices of the inter-chain coupling:

$$\begin{aligned}
c &\leftrightarrow d \\
\Delta_{ij}^I &\leftrightarrow \Delta_{ji}^I
\end{aligned} \tag{A.2}$$

Appendix B. Flow Equation Generators

In the main text we defined 3 different generators the commutator: $\eta = [H_0, J] = \eta_h + \eta_\Delta + \eta_I$ where:

$$\begin{aligned}
\eta_h &= [\hat{J}^c, \hat{h}^c] + [\hat{J}^d, \hat{h}^d] \\
\eta_\Delta &= [\hat{J}^c, \hat{\Delta}^c] + [\hat{J}^d, \hat{\Delta}^d] \\
\eta_I &= [\hat{J}^c + \hat{J}^d, \hat{\Delta}^I].
\end{aligned} \tag{B.1}$$

and presented their form as:

$$\begin{aligned}
\eta_h &= \sum_{ij} F_{ij}^c : c_i^\dagger c_j : + C \leftrightarrow D \\
\eta_\Delta &= \sum_{ijk} \Gamma_{ij|k}^c : n_k^c c_i^\dagger c_j : + F_{ij}^{\Delta^c} : c_i^\dagger c_j : + C \leftrightarrow D \\
\eta_I &= \sum_{ijk} \Gamma_{ij|k}^I : n_k^d c_i^\dagger c_j : + C \leftrightarrow D.
\end{aligned} \tag{B.2}$$

The coefficients F and Γ are given as:

$$\begin{aligned} F_{ij}^c &= J_{ij}^c (\bar{h}_i^c - \bar{h}_j^c) \\ F_{ij}^{\Delta^c} &= 2J_{ij}^c \Delta_{ij}^c (n_i - n_j) \end{aligned} \quad (\text{B.3})$$

and

$$\begin{aligned} \Gamma_{ijk}^c &= 2J_{ij}^c (\Delta_{ik}^c - \Delta_{jk}^c) \\ \Gamma_{ijk}^I &= J_{ij}^c (\Delta_{ik}^I - \Delta_{jk}^I). \end{aligned} \quad (\text{B.4})$$

While the coefficient for the dirty chain can be obtained from the symmetry operation $C \leftrightarrow D$.

Appendix C. The Flow Equations.

The full set of flow equations used in the numerics discussed in the main text is given as:

$$\begin{aligned} \frac{d\bar{h}_k^c}{dl} &= \sum_i 2(J_{ik}^c)^2 [(\bar{h}_k^c - \bar{h}_i^c) + 2\Delta_{ik}^c (n_k^c - n_i^c)] \\ &\quad + 2 \sum_{ij} (J_{ij}^c)^2 (\Delta_{kj}^c - \Delta_{ki}^c) (n_j^c - n_i^c) + \sum_{ij} (J_{ij}^d)^2 (\Delta_{kj}^I - \Delta_{ki}^I) (n_j^d - n_i^d) \\ \frac{dJ_{ij}^c}{dl} &= -J_{ij}^c (\bar{h}_i^c - \bar{h}_j^c)^2 - 2J_{ij}^c \Delta_{ij}^c (n_i^c - n_j^c) (\bar{h}_i^c - \bar{h}_j^c) - \sum_k J_{ik}^c J_{kj}^c (2\bar{h}_k^c - \bar{h}_i^c - \bar{h}_j^c) \\ &\quad - 2 \sum_k J_{ik}^c J_{kj}^c [\Delta_{ij}^c (n_i^c + n_j^c - 2n_k^c) + 2\Delta_{ki}^c (n_k^c - n_i^c) + 2\Delta_{kj}^c (n_k^c - n_j^c)] \\ &\quad - J_{ij}^c (\bar{h}_i^c - \bar{h}_j^c) (n_i^c - n_j^c) (\Delta_{ij}^c + \Delta_{ji}^c) \\ \frac{d\Delta_{ij}^c}{dl} &= 2 \sum_{k \neq i, j, l=i, j} (J_{lk}^c)^2 (\Delta_{ij}^c - \Delta_{kl}^c) \\ \frac{d\Delta_{ij}^I}{dl} &= 2 \sum_k (J_{jk}^d)^2 (\Delta_{ij}^I - \Delta_{ik}^I) + 2 \sum_k (J_{ik}^c)^2 (\Delta_{ij}^I - \Delta_{kj}^I) \end{aligned} \quad (\text{C.1})$$

where $n_k^{c(d)} = \langle n_k^{c(d)} \rangle$ are the densities of the Wick ordered reference state, and the flow for the dirty couplings can be found using the symmetry operation $C \leftrightarrow D$.

Appendix D. Numerical Details

The flow equations are numerically solved using an adaptive step 4^{th} order Runge-Kutta. We work with a clean chain length of 24 sites $\delta N_s = 24$ for a total of 48 sites (32 sites when $\delta = 3$). We control the adaptive step by attempting around 800 discrete Runge-Kutta steps on a log scale from $l = 10^{-3}$ to $l = 10^2$. The adaptive step usually requires additional steps to reach the desired accuracy result in an average number of steps of around 3000.

Since our results requires an accuracy for the couplings on a scale absolute scale 10^{-15} , we devoted careful attention to numerical errors. We found that numerical errors were due to floating-point errors for numbers close to 0 during both the first step and at latter steps. Numerical errors in the first step of a Runge-Kutta approximation are well-known, while the ones at later steps are due to the form of the flow equations. These long time error are due to contributions like $\sum_k J_{ik}J_{kj}(h_i + h_j - h_k)$ that could easily flip sign and cause numerical noise at longer times during the flow.

To manage these errors, we initialized the hoppings J_{ij} for $i \neq j \pm 1$ to ϵ_1 and treated a hopping with $|J_{ij}| < \epsilon_2$ as exactly 0. Choosing $\epsilon_2 > 10^{-15}$ and $\epsilon_1 > \epsilon_2$ was sufficient to reduce floating-point errors to the desired accuracy 10^{-15} . We tested the validity of these numerical approximations by varying ϵ_1 and ϵ_2 and observing no change in the flow.